Indian Journal of Pure & Applied Physics
Vol. 62, July 2024, pp. 553-561
DOI: 10.56042/ijpap.v62i7.8644

Study of High Efficiency Lead Free $FASnI_3$ Perovskite Solar Cell with WO_3ETL and Cu_2O HTL Using Numerical Analysis

Khushboo Dixit & Gufran Ahmad*

Department of Electrical Engineering, Faculty of Engineering, Dayalbagh Educational Institute, Agra 282 005, India

Received 9 February 2024; accepted 20 May 2024

Tin based perovskite solar cell have gained the significant attention in recent year due to its potential to revolutionize the field of photovoltaic. The substitution of lead with tin in perovskite solar cells helps address the toxicity issues associated with lead based material. Formamidinium tin triiodide ($FASnI_3$) had a more solid perovskite structure, wider bandgap of 1.41 eV and is more temperature stable than methylammonium tin triiodide ($MASnI_3$). These are the reasons we chose $FASnI_3$ in this study. In this work we simulated $FASnI_3$ based perovskite solar cell using tungsten trioxide (WO_3) as an electron transport material and cuprous oxide (Cu_2O) as an hole transport material using SCAPS simulation.We investigated the impact of varying the thickness and doping concentration of different layer of PSC. Additionally, the effect of interface defect density and temperature dependence on device performance are examined. Further, various metal back contacts such as Au, Ag, Cu, Pt and Ni are investigated to enhance the power conversion efficiency (PCE) of final structure. The initial design was founded on an reported simulation that achieved the PCE of 14.03 %.The proposed solar cell structure has shown an efficiency of 23.44 % with a Jsc of 22.83 (mA/cm^2), a Voc of 1.18 V, and a FF of 86.95 %. It is the highest reported efficiency of $FASnI_3$ based perovskite solar cell using WO_3 as an ETL till date.

Keywords: Tin based perovskite; Tungsten oxide; Solar cell; SCAPS simulation; Efficiency; Cuprous oxide

1 Introduction

The field of perovskite solar cell has seen rapid advancement in the past few years. Perovskite solar cell is lightweight, flexible and can be engineered to absorb light across a wide range of solar spectrum. Perovskite solar cells possess exceptional intrinsic properties and can be produced using low cost, scalable manufacturing techniques such as solution process[1-4]. The chemical formula of the organic–inorganic perovskite substance is ABX_3. It is composed of three elements: a halide anion (I^-, Br^-, Cl^-, or a combination of these), a divalent metal cation (Sn^{2+} or Pb^{2+}), and a monovalent organic cation (FA^+, MA^+, or Cs^+). Due to their remarkable qualities, methylammonium lead halide perovskite solar cells have attracted a lot of attention from around the world. These characteristics include the ability to be produced using solution-based processes, a high extinction coefficient that facilitates effective absorption of sunlight, an appropriate band gap for efficient conversion of solar energy, and notable advances in power conversion[5-7].

In 2009 group of Japanese scientist led by Miyasaka created the first perovskite solar cell using TiO_2 on Dye-Sensitized Solar Cell. In the press of liquid electrolyte, the stability was very low and the PCE was only 3.8%[8]. In 2011, Park achieved a 6.5% increase in cell efficiency by employing a parallel approach with Quantum dots for monocrystalline materials[9]. To date, perovskite solar cells have a power conversion efficiency (PCE) of more than 25%[10]. Lead-based PSCs were not fully commercialised despite the significant advancements in PCE because of health and environmental concerns due to lead toxicity. As a result, a lot of work has gone into finding non-toxic metals such as tin to replace lead position in perovskite solar cell[11] Sn and Pb belong to the same group and have similarities in their optical and electrical characteristics, tin-based PSCs have demonstrated extremely promising performance. Sn^{2+} is an easy replacement of Pb^{2+} because ionic radius of Sn^{2+}(110 pm) and Pb^{2+}(119 pm) is close to one another[12]. Furthermore, compared to Pb-based perovskites, Sn-based perovskites exhibit comparable or better electrical and optical characteristics, such as longer-lived hot carriers and higher charge carrier mobilities[13]. Sn-based perovskites with an optical bandgap between 1.2 and 1.4 eV have the potential to attain a PCE of about 33%[14,15]. Therefore, Sn is the most likely option

*Corresponding author: (E-mail: gufranahmad@dei.ac.in)

to replace the hazardous lead compound and has a lot of promise for the creation of extremely effective solar cells.

Commonly used tin based perovskite solar cell, $MASnI_3$ (1.3 eV), $CsSnI_3$ (1.3 eV), and $FASnI_3$ (1.41 eV) have lower energy bandgaps than $MAPbI_3$ (1.59 eV), which can maximize photon absorption from incoming sunlight[16].

In 2012 a complete lead free tin based perovskite solar cell was used with efficiency 0.9%[17]. The first research on perovskite solar cells based on $FASnI_3$ was published in 2015 with reported efficiency of 1.41%[18]. In 2016 Lead free Inverted device architecture with a PCE of 6.22% was introduced by using formamidinium tin triiodide as an absorber layer[19]. New method is pioneered for the controlled crystallization of $FASnI_3$, resulting in a material that achieved a photovoltaic conversion efficiency (PCE) of 4.8%[20]. Subsequent advancements by introducing ethylenediammonium doping into $FASnI_3$ led to a notable enhancement in efficiency, reaching 7.14 %[21]. In parallel efforts, A demonstration on significant progress in all inorganic tin-based perovskite solar cells is shown, achieving a promising efficiency milestone of 7.11%[22].

A remarkable power conversion efficiency (PCE) of 10.1% was obtained in 2019 by deploying a novel strategy in which π-conjugated Lewis base molecules was employed to control the formation of grain boundaries during the crystallisation of $HC(NH_2)_2SnI_3$ films[23]. In recent study an excellent efficiency of 11.4 % was obtained by incorporating phenylhydrazine hydrochloride into $HC(NH_2)_2SnI_3$ films to prevent the formation of Sn^{4+} ions which led to the malfunction of the device[24]. In 2020, efficiency of 14.03 % is attainted by SCAPS device simulation study of PSC having $FASnI_3$ as the active layer[25]. In 2023 lead free $FASnI_3$ perovskite nanocrystal is successfully produced by using room temperature synthesis[26].

In this work we employed $FASnI_3$ as a perovskite absorber layer because it is superior semiconductor as compared to $MASnI_3$. $FASnI_3$ has lower bandgap of 1.2-1.4 eV and higher absorption coefficient of 10^5. Most research proved that $FASnI_3$ demonstrated great device performance have higher radiative bi-molecular recombination rate constants, lower Auger recombination, greater carrier mobility and also possess exceptional thermal stability over $MASnI_3$[27]. According to the research done factors responsible for stability difference between $MASnI_3$ and $FASnI_3$ are variations in crystal structure, electronic characteristics, spin-orbit coupling effects, and the interaction between the organic cation and inorganic framework[28].

Tin based PSC is sensitive to the atmosphere due to its low efficiency and simple oxidation issue. According to group of researcher the primary problems include the easy oxidation of Sn^{2+} to Sn^{4+} species, the simple creation of tin vacancies, and the quick deterioration of tin-based perovskites in ambient air[29].

In this work we have used tungsten trioxide (WO_3) as an electron transport layer and cuprous oxide (Cu_2O) as a hole transport layer. Properly designed ETL and HTL layers can help minimize recombination, thus enhancing the overall efficiency of the solar cell. We Chose Cu_2O as an HTL because it is an abundant and ecofriendly material. It has high absorption coefficient ($\sim 10^6$) and low cost of fabrication. WO_3 is used as the electron transport layer because it has strong electron mobility, high conductivity and 80% transmittance in the visible spectrum. Furthermore, WO_3 is inexpensive and simple to fabricate.

2 Methodology for simulation and Structure

2.1 Device structure

In this proposed device configuration, the glass substrate is coated with fluorine-doped tin oxide (FTO) serving as a transparent conductive electrode (TCE). The application of FTO renders the glass substrate low in resistance and highly transparent, allowing incoming light to penetrate. The primary function of the TCE is to facilitate the transmission of light to the photoactive layer, where electron-hole pairs are generated.

The WO_3 ETL (Electron Transport Layer) and FTO layer are combined as a front contact, while the HTL (Hole Transport Layer) Cu_2O is paired with an Au metal electrode to form the back contact. Solar radiation enters the device through the glass side, and the absorber layer absorbs photons, initiating the generation of electron-hole pairs at the junction. To ensure effective separation of oppositely charged carriers, the ETL and HTL function as electron and hole transport layers, respectively.

In this device architecture, a window layer is integrated to prevent carrier recombination at the junction surface, maximizing the generation of electron-hole pairs at the absorber layer junction. Subsequently, under the influence of an external load,

electrons injected into the ETL are transported to the HTL. Thus, the sequence of events within the device encompasses photon absorption, electron-hole pair generation, carrier separation, and the movement of generated carriers. Fig. 1(a & b) shows design configuration of the simulated work.

The current work is carried out using the SCAPS-1D (ver.3.3.07) simulation program, created by the University of Gent in Belgium. The simulations were performed at standard illumination conditions of 1000 W/m^2 and 300 K in the AM 1.5 G spectrum. Seven distinct layers can be used to create a heterostructure solar cell in SCAPS-1D, and simulation can be run in both light and dark environmental conditions[30,31].

The mathematical equations employed in the simulation process include Continuity and Poisson's equations, which are effectively solved by the SCAPS-1D simulator program.

2.1 Simulation Methodology

The initial parameters used in simulation were obtained from multiple theoretical and experimental publications, summarized in Table 1. In this simulation different parameters of the designed solar cell are optimally varied in order to forecast the maximum possible efficiency.

Numerical modelling serves as a powerful tool, employing computer simulations to dissect the intricate behaviors of various systems through the resolution of mathematical equations.

In this context, the SCAPS simulation tool emerges as a cornerstone, facilitating the meticulous numerical analysis and optimization of the proposed heterostructure. Through this precise model, measurements can be thoroughly scrutinized, empowering researchers to gain deeper insights into the performance dynamics of the system.

The SCAPS-1D software was employed to simulate and analyze the J-V characteristics of perovskite solar cells. SCAPS interface offers various actions to choose from, allowing users to select measurements such as band diagram, electron affinity, carrier density, doping concentration, electric field, and the thickness of window, buffer, and absorber layers.

Utilizing the capabilities of the SCAPS simulation software, researchers can delve into a comprehensive analysis encompassing parameters crucial for solar cell performance evaluation. These parameters include power conversion efficiency (PCE), fill factor (FF), short-circuit current, open-circuit voltage, J-V characteristics curve, AC characteristics, and spectral response quantum efficiency (QE).

Table 1 — Basic parameters of each layers used in device simulation[32-35].

Parameters	FTO	WO_3	$FASnI_3$	Cu_2O
W(μm)	0.40	0.04	0.350	0.250
E_g(eV)	3.5	2.6	1.52	2.17
χ (eV)	4.0	3.8	3.53	3.2
Ɛr	9.0	4.8	8.2	7.11
Nc (cm^{-3})	2.2×10^{18}	1×10^{21}	2.2×10^{17}	2.2×10^{17}
Nv (cm^{-3})	1.8×10^{19}	2×10^{20}	1.8×10^{19}	1.1×10^{19}
μ_e (cm^2/V-S)	20	50	2 x 10	2×10^2
μ_p (cm^2/V-S)	10	50	2 x 10	3×10^1
N_D (cm^{-3})	2×10^{19}	2×10^{19}	0	0
N_t (cm^{-3})	10^{15}	10^{15}	10^{15}	10^{15}
N_A (cm^{-3})	0	0	0	1×10^{18}

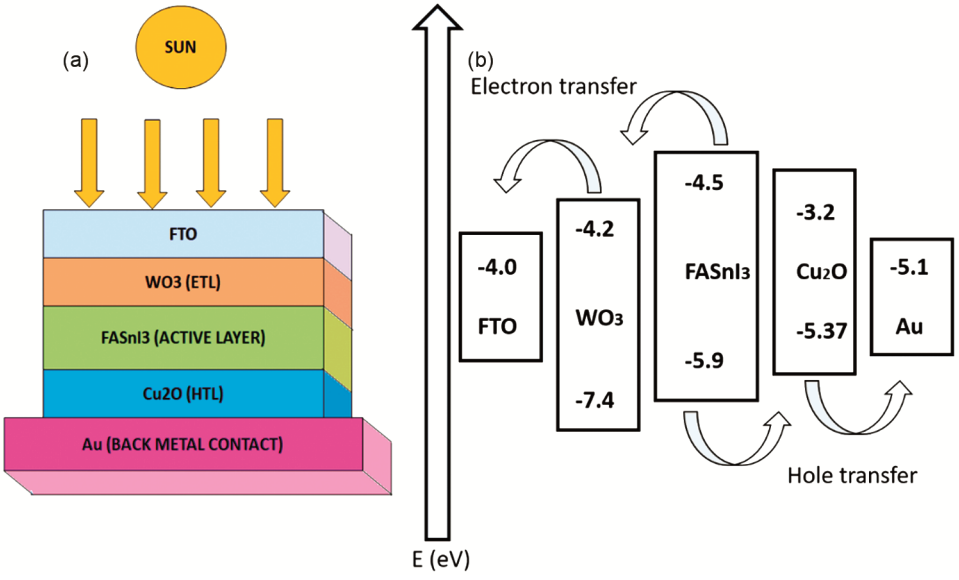

Fig. 1 — (a) device configuration of simulated structure (b) Energy level band diagram

SCAPS-1D simulator program solves fundamental mathematical equations like Poisson's equations and continuity equation.Where n(x) and p(x) are trapped hole and electron density. Donor density and acceptor density is denoted by N_D and N_A respectively.

$$\frac{d}{dx}\left(-\varepsilon(x)\frac{d\varphi}{dx}\right) = [p(x) - n(x) + N_D(X) - N_A(x) + p(x) - n(x)] \quad \ldots(1)$$

One dimensional continuity equation for electrons and holes are as follows

$$\frac{\partial n(x,t)}{\partial t} = \frac{1}{q}\frac{\partial Jn}{\partial x} + G_n(x,t) - R_n(x,t) \quad \ldots(2)$$

$$\frac{\partial p(x,t)}{\partial t} = \frac{1}{q}\frac{\partial Jp}{\partial x} + G_p(x,t) - R_p(x,t) \quad \ldots(3)$$

Carrier density for electrons and holes are

$$J_n = q\left(n\mu_n E + D_n\frac{dn}{dx}\right) \quad \ldots(4)$$

$$J_p = q\left(p\mu_p E + D_p\frac{dp}{dx}\right) \quad \ldots(5)$$

In steady state conditions $\frac{dn}{dt} = 0$, Hence

$$\frac{1}{q}\frac{\partial J_n}{\partial x} = -G_n(x,t) - R_n(x,t) \quad \ldots(6)$$

On substituting the value of j_n from the above equation we get

$$n\mu_n\frac{dE}{dx} + E\mu_n\frac{dn}{dx} + D_n\frac{d^2n}{dx^2} = -G_n(x,t) - R_n(x,t) \quad \ldots(7)$$

Similarly for holes

$$-p\mu_p\frac{dE}{dx} - E\mu_p\frac{dp}{dx} + D_p\frac{d^2p}{dx^2} = -G_p(x,t) - R_p(x,t) \quad \ldots(8)$$

These coupled differential equations are solved by SCAPS, to find the unknown variables.

3 Results and discussion

3.1 The effect of varying absorber layer thickness

The fundamental parameters used to run the SCAPS simulation are listed in Tables 1 & 2. In this work we are varying the thickness of $FASnI_3$ absorber layer from 100 nm to 700 nm. Fig. 2. shows the impact of thickness variation on the performance parameters. Voc, Jsc, FF and PCE is varying in range (1.183-1.174 V), (14.04-23.6 mA/cm^2), (87.40-86.12 %) and (14.54-25.53%) respectively. Absorber layer thickness plays a crucial role in determining its performance of perovskite solar cell.

Variations in absorber thickness notably affect the short-circuit current density (J_{SC}) of the device. This is primarily because the thickness of the absorber determines the absorption of incident light, which in turn regulates the density of photo-generated carriers. Thus, investigating the influence of absorber thickness on device performance is crucial for optimizing its efficiency. Quality of absorber layer is a crucial parameter for determining the carrier lifetime within the active region of solar cells, If the diffusion length is short generated carriers within the bulk are prone to recombine prematurely, diminishing the overall performance of solar cells. Relation between carrier lifetime and diffusion length is given by Eq. 9.[39]

$$L_{n\,(p)} = \sqrt{\tau_{n\,(p)} D_{n\,(p)}} \quad \ldots(9)$$

Here, Ln(p) represents the electron (hole) diffusion length, τn(p) denotes the electron (hole) lifetime, and Dn(p) signifies the electron (hole) diffusion coefficient.

From the obtained graph shown in Fig. 2. it is observed that when absorber layer thickness is less (50 nm- 150 nm) lower value of Jsc is obtained. It has been observed that Jsc increases with increase in absorber layer thickness because it enhances the light's absorption, consequently leading to a rise in

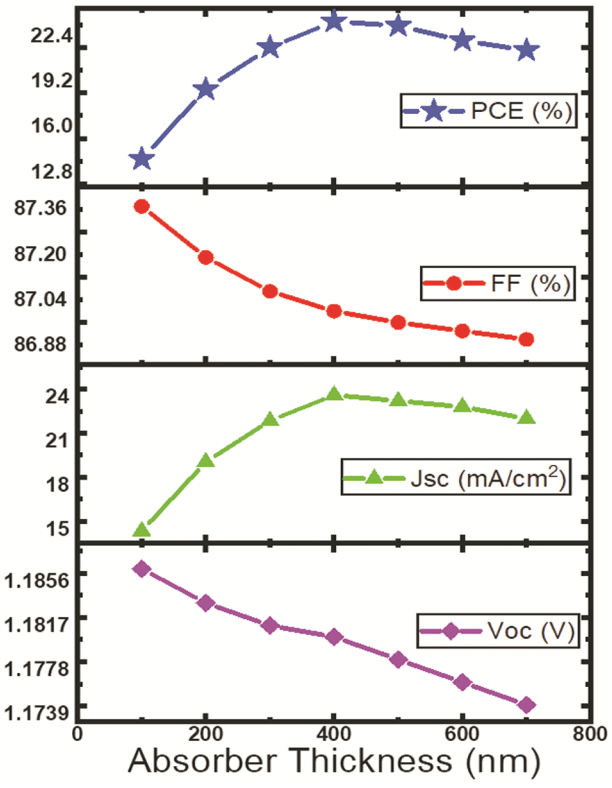

Fig. 2 — Variation of PCE of perovskite solar cell on the basis of absorber layer thickness

J_{SC}. However, when the absorber thickness is increased from 250-350 nm, the effect on J_{SC} becomes negligible. This is due to the absorber thickness surpassing the space charge region and creating a quasi-neutral zone where carrier recombination probability escalates significantly. Consequently, despite the increased light absorption from the thicker absorber, J_{SC} remains stable due to the augmented bulk recombination, which counteracts the surplus carriers generated.

Moreover, as the absorber thickness exceeds 400 nm, J_{SC} starts to decrease. Jsc reached to its maximum value 23.6 mA/cm^2 at 400 nm thickness of absorber layer. After 400 nm thickness Jsc starts decreasing. This decline occurs because bulk recombination starts to dominate over the enhanced carrier generation facilitated by the thicker absorber FF is continuously decreasing with increase in absorber layer thickness from 1.183 V to 1.174V. Voc is gradually decreasing with increase in absorber layer thickness due to increase in series resistance within the solar cell. The open circuit voltage is influenced by the diffusion length of charge carriers within the material. If the absorber layer is too thick carriers may not be able to reach the contacts before recombining, resulting in a decrease in the open circuit voltage.

As the thickness of the perovskite solar cell increases significantly, there's a noticeable decrease in the open-circuit voltage (V_{OC}). This decrease in V_{OC} is directly related to both the short-circuit current (J_{SC}) and the reverse saturation current (J_O), as indicated in Eq. 10. These parameters depend on the thickness of the perovskite layer, where V_t represents the thermal voltage[40].

$$V_{oc} = V_t \ln \frac{Jsc}{Jo} + 1 \quad \ldots (10)$$

So, we need to find an optimal thickness for the absorber layer that balances light absorption, carrier generation and collection efficiency. In this simulated work the optimum thickness is achieved at 350 nm.

3.2 The effect of varying ETL and HTL thickness

In this work thickness of ETL is varied from 10 nm to 60 nm and thickness of HTL is varied from 100 to 400 nm using SCAPS-1D simulating tool. We are using WO_3 as an ETL because it possesses good electron mobility. Primary function of an ETL is to block holes and transport electrons efficiently from absorber layer to the cathode. While varying the thickness of ETL and HTL the absorber layer thickness is kept on its optimum value attained in the previous section. Other parameters are taken from Table 1 & 2.

Initially the thickness of WO_3 is varied by keeping thickness of HTL and absorber layer constant. From Fig. 3(a) we can infer the effect of ETL thickness on the PCE of perovskite solar cell. If the thickness of ETL is less than 15 nm the electrons may not be effectively collected and transported leading to lower Jsc. On the other hand an excessive thick ETL may introduce resistance and hinder charge transport results in lower PCE. It can be observed that there is only a significant, slight variation observed in the Jsc, Voc, and %FF values. Voc and Jsc is decreasing in range (1.1806-1.1801 V) and (22.834-22.827 mA/cm^2) respectively. This is primarily due to the uniform number of charge carriers produced in the lead-free perovskite material, and the significant decrease in the %PCE values may be due to more charge recombination at the ETL/Absorber interface. The optimal thickness of ETL in this simulation is 40 nm.

Table 2 — Defect density parameters at interface of device[36-38].

Parameters	ETL/$FASnI_3$	$FASnI_3$/HTL
Type of defects density	Neutral	Neutral
Defect density N_t (cm^{-3})	1 x 10^{16}	1 x 10^{16}
Energy distribution	Single	Single
Reference energy (eV)	0.6	0.5
Level of energy relative to Ev	Above the highest Ev	Above the highest Ev
Cross section area of electron (cm^2)	1 x 10^{15}	1 x 10^{15}
Cross section area of hole (cm^2)	1 x 10^{15}	1 x 10^{15}

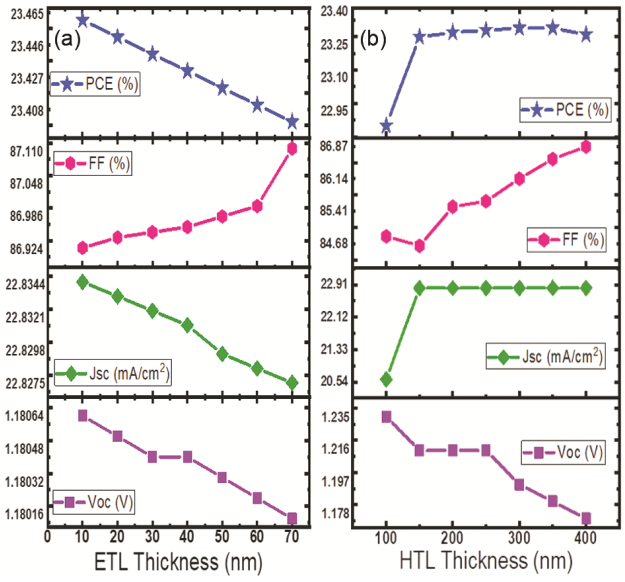

Fig. 3 — (a) Impact of ETL thickness on the performance of solar cell (b) Impact of HTL thickness on the performance of solar cell

Now thickness of Cu_2O is varied from 100 to 400 nm by keeping all the other parameters constant. Fig. 3(b) Plots shows that when the thickness of the HTL increases from 100-400 nm, Jsc increases from 20.61 mA/cm^2 to 22.83 mA/cm^2, virtually reaching a constant value. Increasing the thickness of the HTL can lead to an increase in optical absorption within the layer, resulting in a higher generation rate of electron-hole pairs. This can lead to an increase in Jsc up to a certain point. It was found that increasing thickness also reduced the open circuit voltage (Voc) from 1.23 V to 1.17 V. Adjusting the HTL thickness can affect the energy level alignment at the interfaces and the charge transport properties within the device due to energy level mismatches and charge carrier recombination, Voc is falling.In this work the optimal thickness of the HTL is 250 nm.

3.3 The effect of varying doping concentration and Interface defect density

The potential oxidation of Sn^{2+} to Sn^{4+} leads to heightened defect density within $FASnI_3$. These defects serve as recombination centers within the bulk layer, adversely impacting key device performance parameters such as open-circuit voltage and fill factor (FF). In the absorber layer of PSCs, three types of simultaneous recombination—radiative, Auger, and Shockley-Read-Hall (SRH) is explained through Eq. 11.

$$R_{(Bulk)} = R_{(Auger)} + R_{(Radiative)} + R_{(SRH)} \quad \ldots (11)$$

In the given equation, R_{SRH} denotes the rate of Shockley-Read-Hall (SRH) recombination. For P-type material standard SRH model is given by Eq. 12[41,42].

$$R_{SRH} = \frac{pn - n_i^2}{\tau_p\,(n_1 + \Delta n) + \tau_n\,(N_A + p_1 + \Delta n)} \quad \ldots (12)$$

The variables p and n denote the concentrations of holes and electrons, respectively, while τ_p and τ_n represent the lifetimes of these charge carriers. Additionally, n_i represents the intrinsic concentration of charge carriers. Carrier concentration is denoted by Δn.

$$n_1 = N_C \exp\left(\frac{E_{trap} - E_C}{kT}\right) \quad \ldots (13)$$

$$p_1 = N_v \exp\left(\frac{E_v - E_{trap}}{kT}\right) \quad \ldots (14)$$

E_C and E_V represent the edges of the conduction and valence bands respectively, while N_C and N_V denote the density of states in the conduction and valence bands. Etrap stands for the energy level of defects, and T represents the operating temperature. Auger recombination is expressed in Eq. 15[43].

$$R_{(Auger)} = (A_n n + A_p)(np - n_i^2) \quad \ldots (15)$$

Auger recombination is calculated under the assumption of charge carrier balance, where electron density (n) equals hole density (p), with a coefficient $A_n = A_p = 9.3 \times 10^{-30}$ cm^6/s [24]. Radiative recombination is expressed through Eq. 16[44].

$$R_{(Radiative)} = B\,(np - n_i^2) \quad \ldots (16)$$

Here, B represents the coefficient for radiative recombination, equivalent to 2×10^{-10} cm^3/

In First part of this section numerical simulation has been performed to demonstrate how interface defect density affects PCE curves for both interface layers (WO_3/$FASnI_3$ and $FASnI_3$/Cu_2O) of an optimized $FASnI_3$ solar cell. From Fig. 4(a) it is observed that voltage failure is observed when the interface defect density surpasses 1.0×10^{14} cm^{-3}. Interface defect density can acts as a recombination centers leading to a reduction in Voc. Lower Voc directly translates in lower power conversion

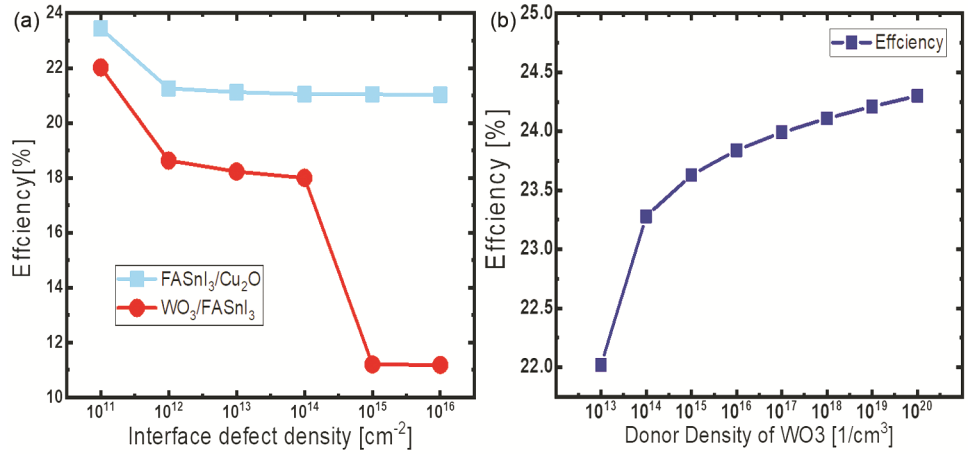

Fig. 4 — (a) Impact of interfacial defects WO_3/$FASnI_3$ and $FASnI_3$/Cu_2O on PCE of solar cell (b) Impact of donor density of WO_3 on the PCE

efficiency. Higher interface defect density can increase the resistance of charge carrier transport leading to low Jsc. Interface defects can influence the FF of solar cell by affecting both Jsc and Voc. Cell performance is negatively impacted by larger defect density of the two interfaces which also bring additional trap and recombination centers. Thus, the simulation findings show that the ideal interface defect density for device simulation is 1×10^{10} cm^{-3}. It has been observed that WO3/FASnI3 heterointerface is showing a sudden decrement in the efficiency after $1x10^{14}$ $/cm^2$ but same behavior is not observed in the interface defects at the $FASnI_3/Cu_2O$ heterointerface because the ETL/perovskite interface serves as both a light-facing interface and a radial interface, amplifying its effect on performance compared to the HTL/perovskite interface. Electrons typically have higher mobility in organic materials compared to holes. This means that defects in the ETL layer can more readily impede electron transport, leading to a more significant impact on device performance compared to defects in the HTL layer. The energy level alignment at the interfaces plays a crucial role in charge injection and extraction. Defects in the ETL layer can disrupt this alignment more significantly than in the HTL layer, impacting charge carrier injection and device performance.

In second partof this section we have analyzed the effect of donor doping density (N_D) of electron transport layer on the performance of perovskite solar cell. We have varied the doping density of WO_3 layer from 1 x 10^{13} to 1 x 10^{20} cm^{-3} while other parameters are kept unchanged. We can infer from Fig. 4(b) that all the four parameters (Voc, Jsc, PCE, and FF) increased with increasing donor density. Low doping concentrations result in decreased conductivity and increased charge carrier recombination, which lowers Voc, Jsc, FF, and PCE. At a donor doping concentration of $1 \times 10^{20} cm^{-3}$, the maximum values of Voc, Jsc, FF, and PCE were obtained as 1.20 V, 22.832 mA/cm^2, 88.56, and 24.30%, respectively. The donor density of ETL influences the availability of charge carriers for transport. Higher N_D can lead to better electron transport properties reducing the likelihood of charge carriers being trapped or lost within the ETL. This can contribute to improved charge transport efficiency and results in higher power conversion efficiency. Our simulation results indicate that optimised doping concentration for ETL and HTL is $1x10^{19}$ cm^{-3}

3.4 effect of back contact work function

In this section we have simulated and compared the various metal back contacts that we employed in our work. Metal contacts are crucial for improving PSC efficiency. We compare them to see which one works best with our $FASnI_3$ based perovskite solar cell. We determine which metal contact has a high efficiency and is suitable for use as a metal contact for the design simulation cell. Here we used silver, platinum, gold, nickel and copper as a back contact. We got highest PCE of 23.48 %at the platinum design cell. Lowest efficiency of 19.95 % is obtained by using silver as a back metal contact. We have used Au as a metal back contact in this simulation Fig. 5.

3.5 The effect of varying temperature

In this work, temperature of solar cell operation has been successfully varied from 300K to 400K. The observed result is shown in Fig. 6. We observed that

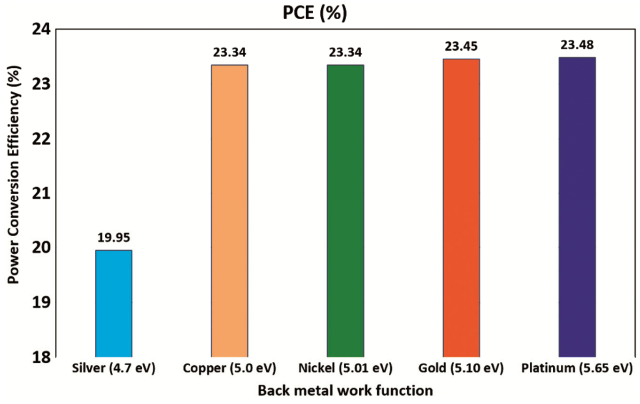

Fig. 5 — Impact of work function of different metal back contact on the PCE of perovskite solar cell

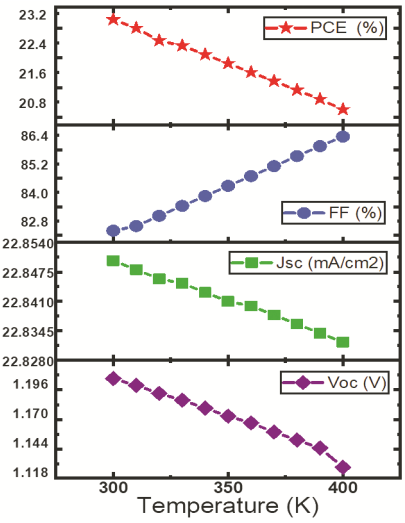

Fig. 6 — Impact of temperature on the PCE of perovskite solar cell

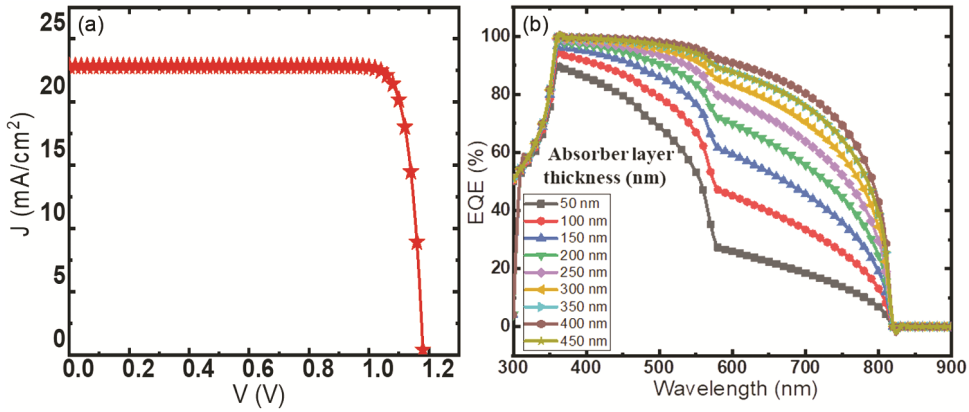

Fig. 7 — (a) final optimized J-V curve of perovskite solar cell (b) EQE plot as a function of wavelength for different thickness of absorber layer

Table 3 — Comparison of present work with experimental and theoretical literature.

Parameters	Experimental [18]	Reported Simulation [25]	Presented Work
Voc (V)	0.264	0.92	1.18
Jsc (mA/cm^2)	15.85	22.65	22.83
FF (%)	42	67.74	86.95
PCE (%)	1.75	14.03	23.44

the efficiency of solar cell is gradually decreasing with increasing the temperature. The performance of perovskite solar cells is significantly influenced by temperature. This is primarily due to increased charge carrier recombination rates and reduced carrier mobility. Perovskite solar cell exhibit peak efficiency at low temperature, extreme temperature can negatively affect their performance.

We achieve the highest Voc at 300 K and it further declined with rise in temperature.Jsc is decreasing gradually from 22.85 to 22.83 mA/cm^2. Fill factor is increasing gradually from 83 to 86.95 % with increase in temperature.

3.6 Analysis of result

In the current work, we utilized Sn material for that purpose because it has qualities that are similar to those of Pb and is also environment friendly and non-toxic in nature. The Table 3 is showing the comparison among the parameters of the proposed device structure with previously reported experimental[25] and simulated paper[18]. The optimized results together indicate that optimizing the absorber's thickness, the ETL and HTL's affinity, and both play a critical role in improving the cell's performance.

In Fig. 7(a) we are showing the final optimized J-V curve of our simulated structure of $FASnI_3$ based perovskite solar cell. In Fig. 7(b). The external quantum efficiency (EQE) of a solar cell is plotted with respect to absorber thickness varied from 50 nm to 450 nm. EQE is increasing initially and after a certain point it is falling because a thicker absorber layer generally allows for more absorption of photons, increasing the likelihood of generating electron-hole pairs and thus contributing to a higher EQE. When the thickness is increased beyond 400 nm EQE starts decreasing because if the absorber layer is too thick, it may lead to increased carrier recombination before carriers can be collected. Optimal absorber layer thickness is 350 nm.

4 Conclusion

In the present work, we have inspected the planer n-i-p structure of device model FTO/WO_3/$FASnI_3$/Cu_2O/Au. Numerous studies are previously conducted on non-toxic ecofriendly $FASnI_3$ absorber layer, they demonstrated low power conversion efficiency. In this study, $FASnI_3$ devices were simulated to explore the impact of different device parameters like thickness, temperature, back contact, concentration of doping and interface defect density on their performance. The simulation results indicate that the primary reason for the inadequate performance of these devices is attributed to the self-oxidation of positively charged tin ion. In this work lead free formamidinium tin based perovskite solar cell was optimized and examined in a systematic manner to attain the highest PCE using SCAPS simulation. In this work we utilized Cu_2O as HTL and WO_3 as ETL. The reported optimal thickness of the HTL, ETL, and Absorber layers is 250 nm, 40 nm, and 350 nm respectively. Electron affinity of ETL and HTL, Capture cross section were also considered and optimized. After using the same methodology to all of our work, we were able to achieve PCE a 23.44 %, Jsc (22.83 mA/cm^2), FF (86.95 %), and Voc (1.8 V). It is concluded that

parameters associated with the ETL and Hole Transport Layer HTL play a crucial role in determining the overall performance of device. Furthermore, our simulation results indicate that optimised doping concentration for ETL and HTL is $1x10^{19}$ cm^{-3}.

We have also analysed the effect of interface defect density on the performance of solar cell. The analysis revealed that interface defect density significantly influences charge transport and recombination, underscoring the importance of defect minimization for enhancing device efficiency. The defect density must below 1 x 10^{10} cm^{-2} for good efficiency. It has been found that ETL/Absorber interface defects have significant impact on performance of solar cell as compared to Absorber/HTL interface. Finally, the effect of temperature on device performance was also observed revealing the outcome that indicates PCE is temperature sensitive. PCE is noticeable at lower temperature and gradually deteriorates as the temperature rises, best performance of the device is noticed at 300K. We also analyzed the effect of different metal back contact and concluded that platinum is giving the highest efficiency as compare to other metals contact. Final obtained results are also compared with the published work. The reported efficiency is the highest efficiency of $FASnI_3$ based solar cell using WO_3 as an ETL till date.

References

1 Noh J H, Im S H, Heo J H, Mandal T N & Seok I S, *Nano Lett*, 13 (2013) 1764.
2 De W S, Holovsky J, Moon S J, Loper P, Niesen B, Ledinsky M, Haug F J,Yum J H & Ballif C, *J Phys Chem Lett*, 5 (2014) 1035.
3 Anwer S S A, Kumar M & Das M K, *Semicond Sci Technol*, (2018). https://doi.org/10.1088/1361-6641/aadf71.
4 Dong Q, Fang Y, Yuchuan S P, Mulligan J, Qiu L C, Huang J, *Sci Express*, 43210 (2015) 1.
5 Sun W, Li Y, Ye S, Rao H, Yan W, Peng H, Li Y, Liu Z, Wang S, Chen Z, Xiao L, Bian Z & Huang C, *Nanoscale*, 8 (2016) 10806.
6 Momblona C, Gil-Escrig L, Bandiello E, Hutter E M, Sessolo M, Lederer K, Blochwitz-Nimoth J, Bolink H J, *Energy Environ Sci*, 9 (2016) 3456.
7 Askari S S A, Kumar M & Das M K, *Mater Today Proc*, 4 (2017) 12647.
8 Kojima A, Teshima K, Shirai Y, Miyasaka T, *J Am Chem Soc*, 131 (17) (2009) 6050.
9 Serrano-Lujan L, Espinosa N, Larsen-Olsen T T, Abad J, Urbina A, F C Krebs, *Adv Energy Mater*, 5 (2015) 1501119.
10 Yoo J J, Shin S S, Seo J, *ACS Energy Lett*, 7 (2022) 2084.
11 Yan Y, Pullerits T, Zheng K & Liang Z, *ACS Energy Lett*, 5 (2020) 2052.
12 Zhou Y, Saliba M, *ACS Energy Lett*, 6 (2021) 2750.
13 Nishimura K, Kamarudin M A, Hirotani D, Hamada K, Shen Q, Iikubo S, Minemoto T, Yoshino K & Hayase S, *Nano Energy*, 74 (2020).
14 Jiang X, Zang Z, Zhou Y, Li H, Wei Q, Ning Z, *Accounts Mater Res*, 2 (2021) 210.
15 Tai Q, Guo X, Tang G, You P, Ng T W, Shen D, Cao J, Liu C K, Wang N, Zhu Y, Lee C S & Yan F, *Angew Chem Int E Engl*, 58 (2019) 806.
16 Tao S, Schmidt I, Brocks G, Jiang J, Tranca I, Meerholz K & Olthof S, *Nat Commun*, 10 (2019) 2560.
17 Joy S, Atapattu H R, Sorensen S, Pruett H, Olivelli A B, Huckaba A J, Miller A-F & Graham K R, *J Mater Chem A*, 10 (2022) 13278.
18 Koh T M, Krishnamoorthy T, Yantara N, Shi C, Leong W L, Boix P P, Grimsdale A C, Mhaisalkar, S G & Mathews N, *J Mater Chem A*, 3 (2015) 14996.
19 Liao W, Zhao D, Yu Y, Grice C R, Wang C, Cimaroli A J, Schulz P, Meng W, Zhu K, Xiong R G, & Yan Y, *Adv Mater*, 28 (2016) 9333.
20 Lee S J, *et al*., *J Amer Chem Soc*, 138 (2016) 3974.
21 Ke W, *et al*., *Sci Adv*, 3 (2017) e1701293.
22 Chen M, *et al*., *Nature Commun*, 10 (2019) 1.
23 Wu T, Liu X, He X, Wang Y, Meng X, Noda T, Yang X, Han L, *Sci China Chem*, 63 (2020) 107
24 Wang C, Gu F, Zhao Z, Rao H, Qiu Y, Cai Z, Zhan G, Li X, Sun B, Yu X, Zhao B, Liu Z & Bian Z, Huang C, *Adv Mater*, 32 (2020) 1.
25 Abdelaziz S, Zekry A, Shaker A & Abouelatta M, *Opt Mater (Amst)*, 101 (2020) 109738.
26 Chen Z & Tara P D, *Appl Phys Rev*, 10 (2023) 011404. https://doi.org/10.1063/5.0125100.
27 Gu F, Ye S, Zhao Z, Rao H, Liu Z, Bian Z & Huang C, *Sol RRL*, 2 (2018) 1.
28 Peng L & W Xie, *RSC Adv*, 10 (2020) 14679.
29 Noel N K, Stranks S D, Abate A, Wehrenfennig C, Guarnera S, Haghighirad A-A, Sadhanala A, Eperon G E, Pathak S K, Johnston M B, Petrozza A, Herz L M & Snaith H J, *Energy Environ Sci*, 7 (2014) 3061.
30 Rai S, Pandey B K & Dwivedi D K, *Opt Mater (Amst)*, 100 (2020) 109631.
31 Burgelman M, Nollet P, Degrave S, *Thin Solid Films*, 361 (2000) 527.
32 Hossain M I, Alharbi F H & Tabet N, *Sol Energy*, 120, (2015) 370.
33 Rai N, Rai S, Singh P K, Lohia P & Dwivedi D K, *J Mater Sci Mater Electron*, 31 (2020) 16269.
34 Shukla R R, Kumar D, Punetha & Pandey S K, *IEEE J Photovolt*, 13 (2023) 404.
35 DeepthiJayan K & Sebastian V, *Solar cell*, (2021). http://dx.doi.org/10.1016/j.solener.2021.01.058
36 Sadanand D D K, *Opt Mater (Amst)*, 109 (2020) 11040.
37 Hima A, Lakhdar N, Benhaoua B, Saadoune A, Kemerchou I & Rogti F, *Superlattice Microst*, 129 (2019) 240.
38 Kumar A & Kumar M & Raj A, *Opt Mater*, (2020). 108.
39 Raghvendra R, Kumar R & Pandey S K, *2019 IEEE 46th Photovoltaic Specialists Conference (PVSC)*, Chicago, IL, USA, (2019) 1191.
40 Raghvendra R Kumar R & Pandey S K, *J Electron Mater*, 51 (2022) 6603.
41 Sherkar T S, Momblona C, Gil-Escrig L, Avila ´J, Sessolo M, Bolink H J & Koster L J A, *ACS Energy Lett*, 2 (2017) 1214.
42 Shukla D P, R Kumar & Pandey S K, *Opt Mater*, 143 (2023) 114124.
43 Shukla R, R Kumar & S K Pandey, *IEEE Trans Electron Dev*, 68 (2021) 3446.
44 Bhatt R, Shukla C, Pathak S & Pandey K, *Solar Energy*, 215 (2021) 473.